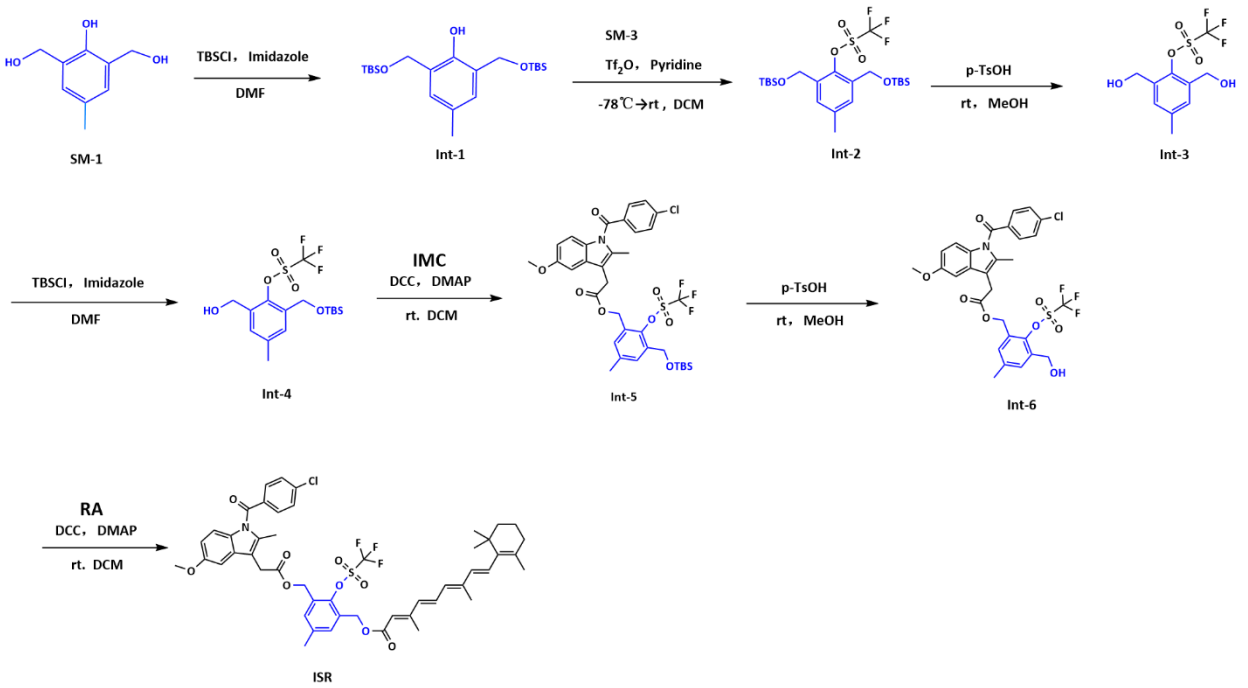

Scheme S1 The synthetic route of ISR.

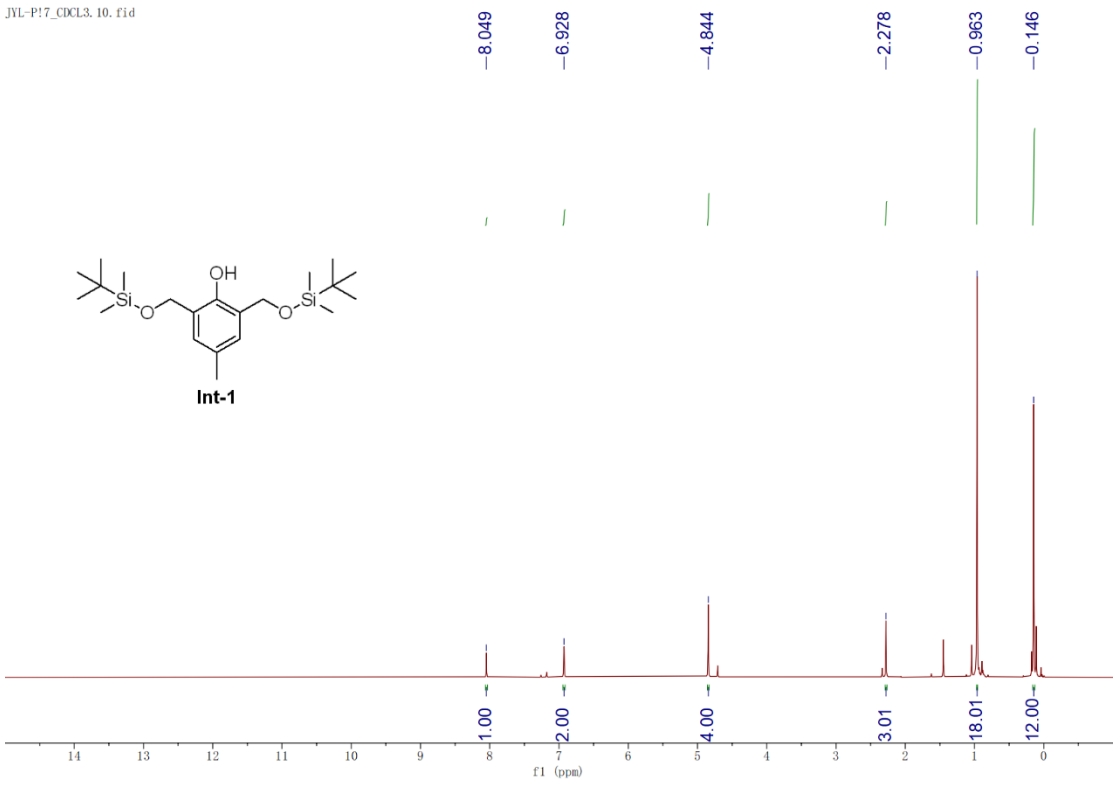

Figure S1 ^{1}H NMR spectrum of Int-1.

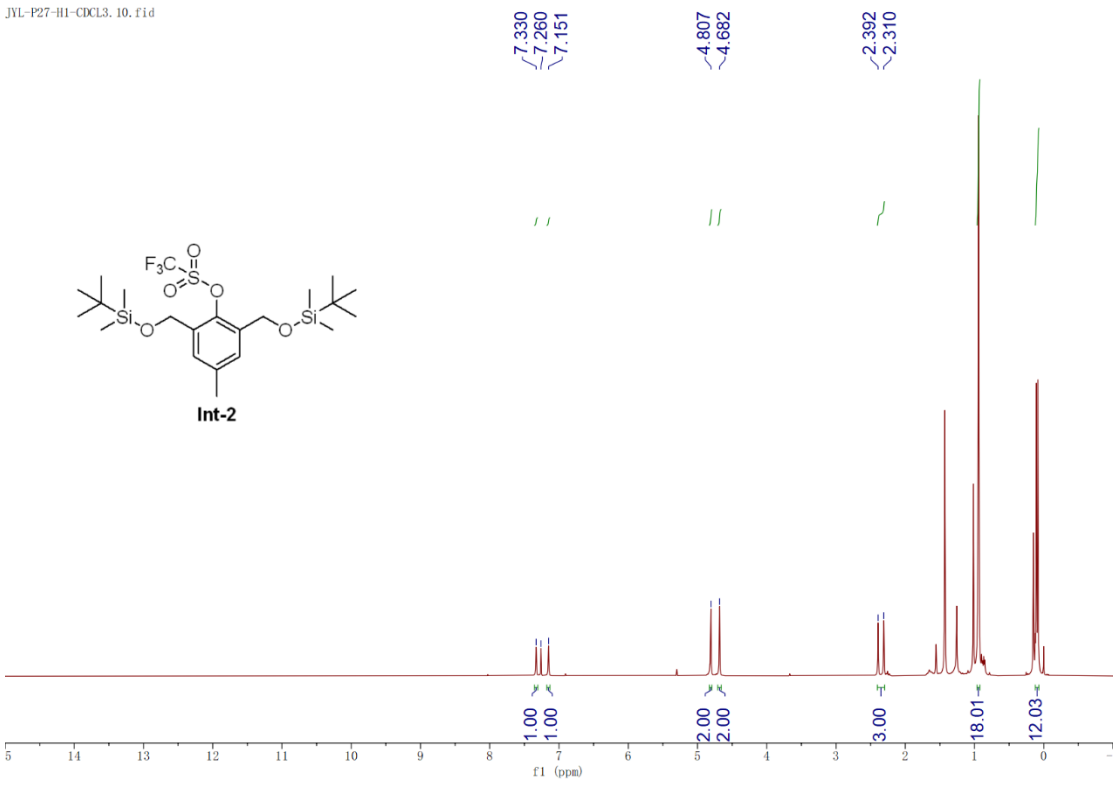

Figure S2 ^{1}H NMR spectrum of Int-2.

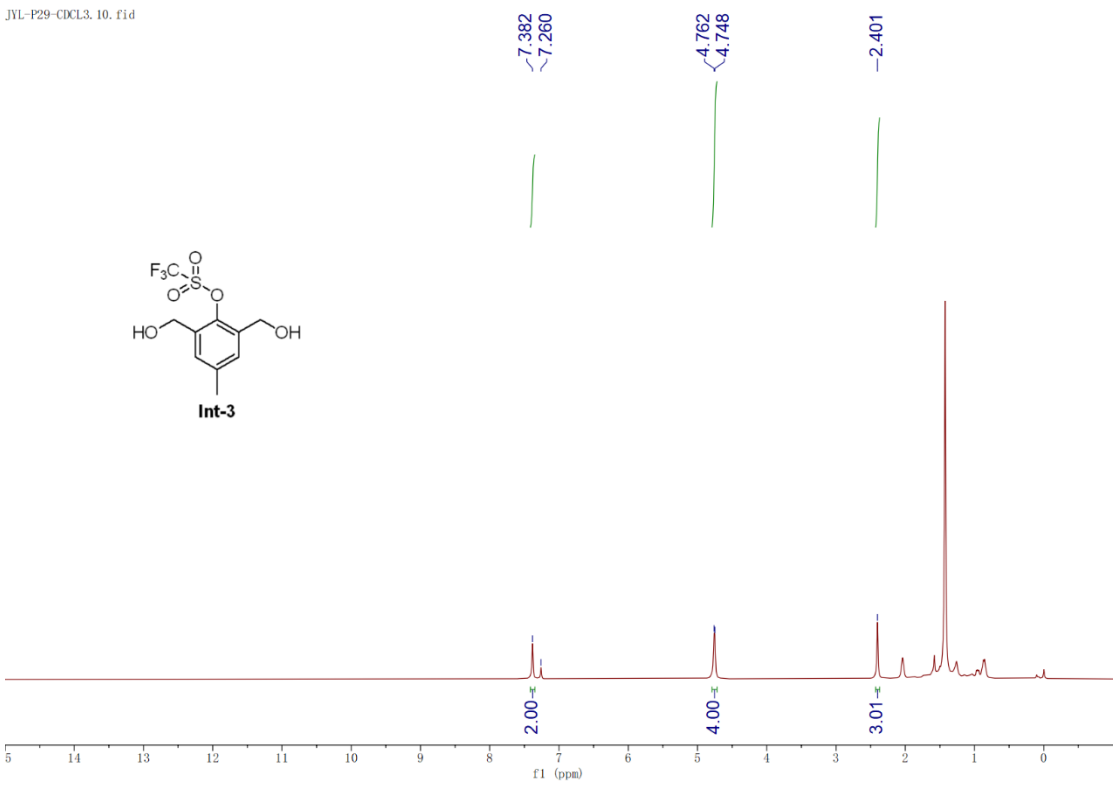

Figure S3 ^{1}H NMR spectrum of Int-3.

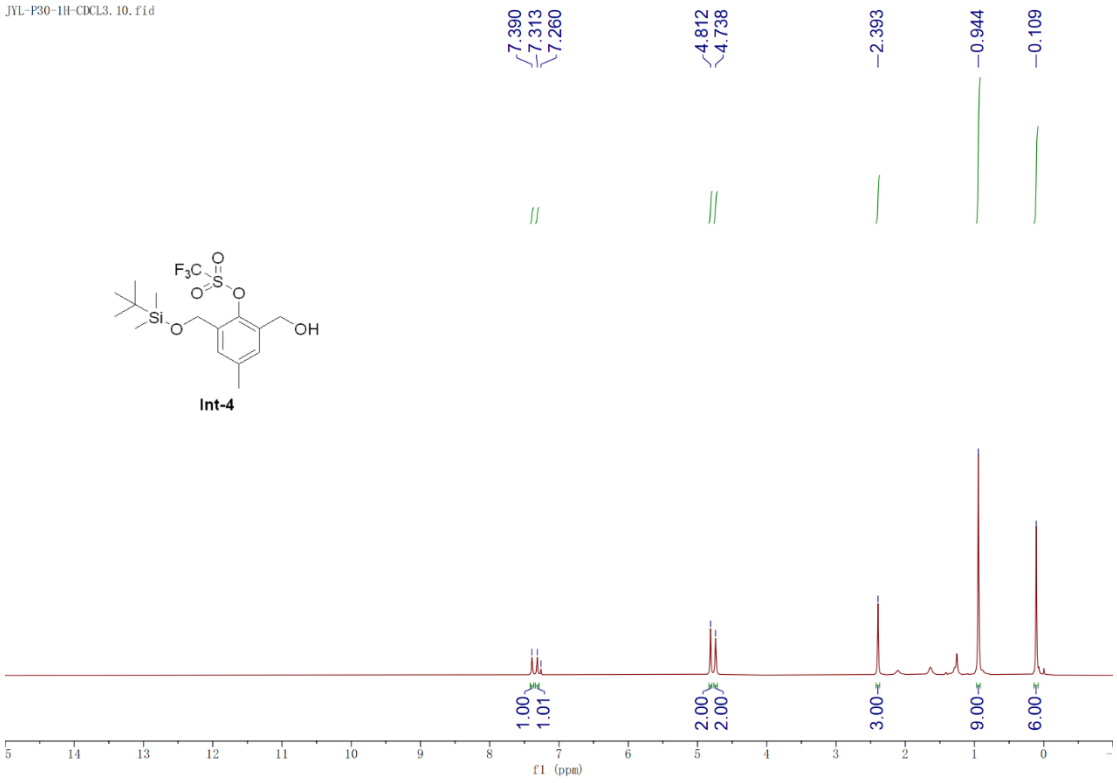

Figure S4 ^{1}H NMR spectrum of Int-4.

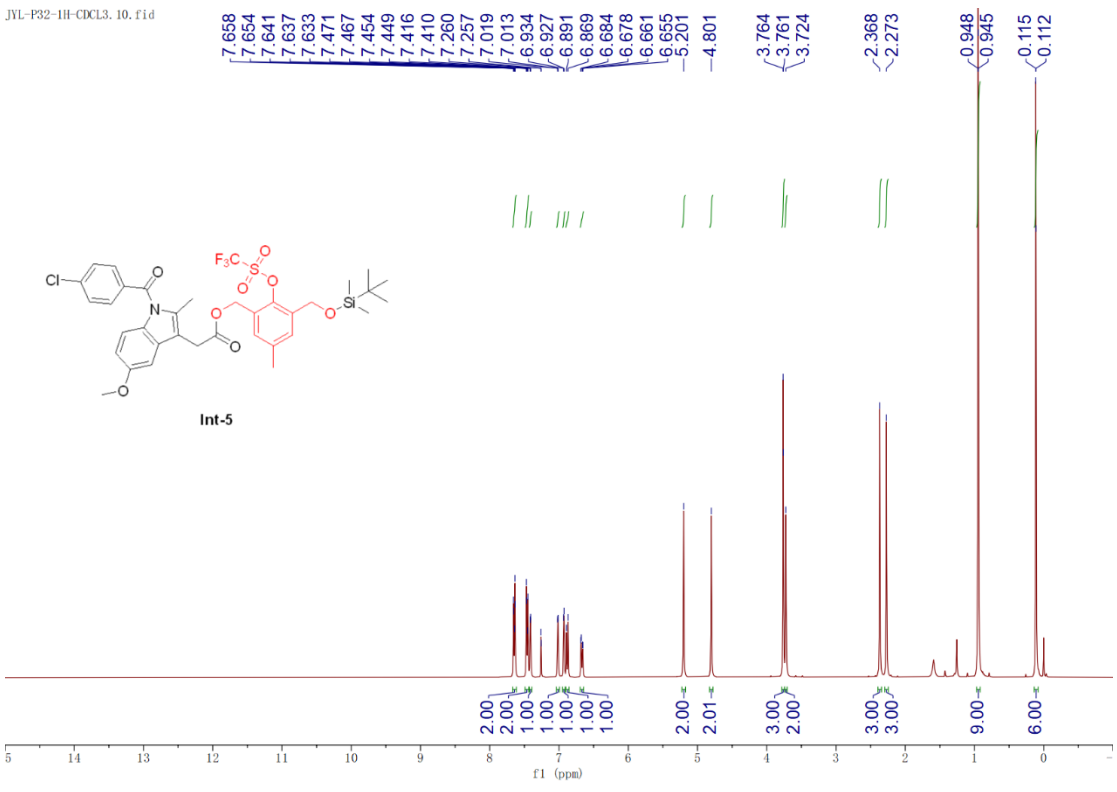

Figure S5 ^{1}H NMR spectrum of Int-5.

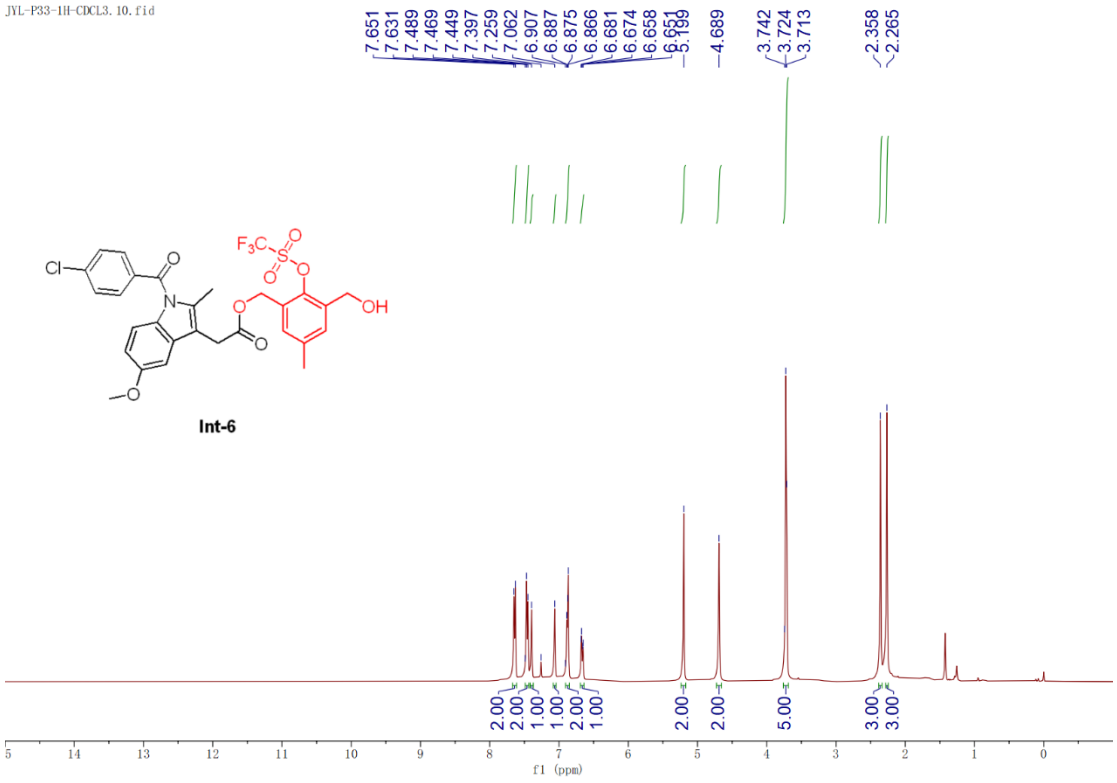

Figure S6 ^{1}H NMR spectrum of Int-6.

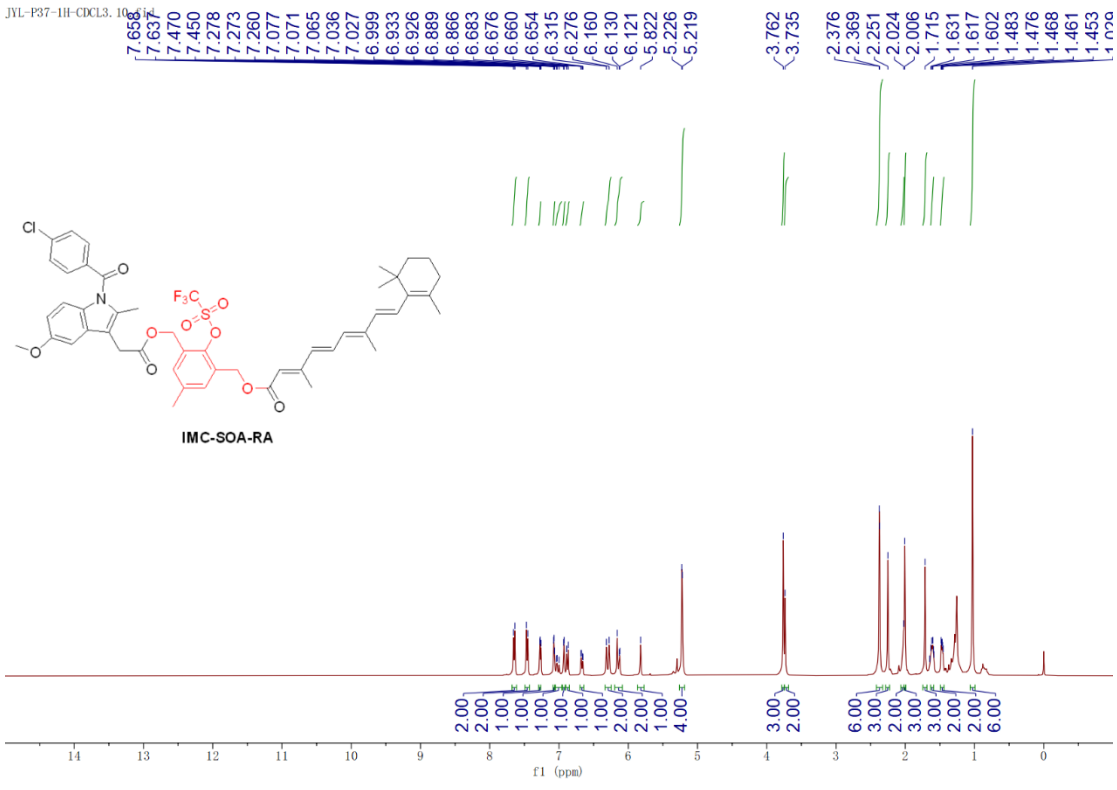

Figure S7 ^{1}H NMR spectrum of ISR.

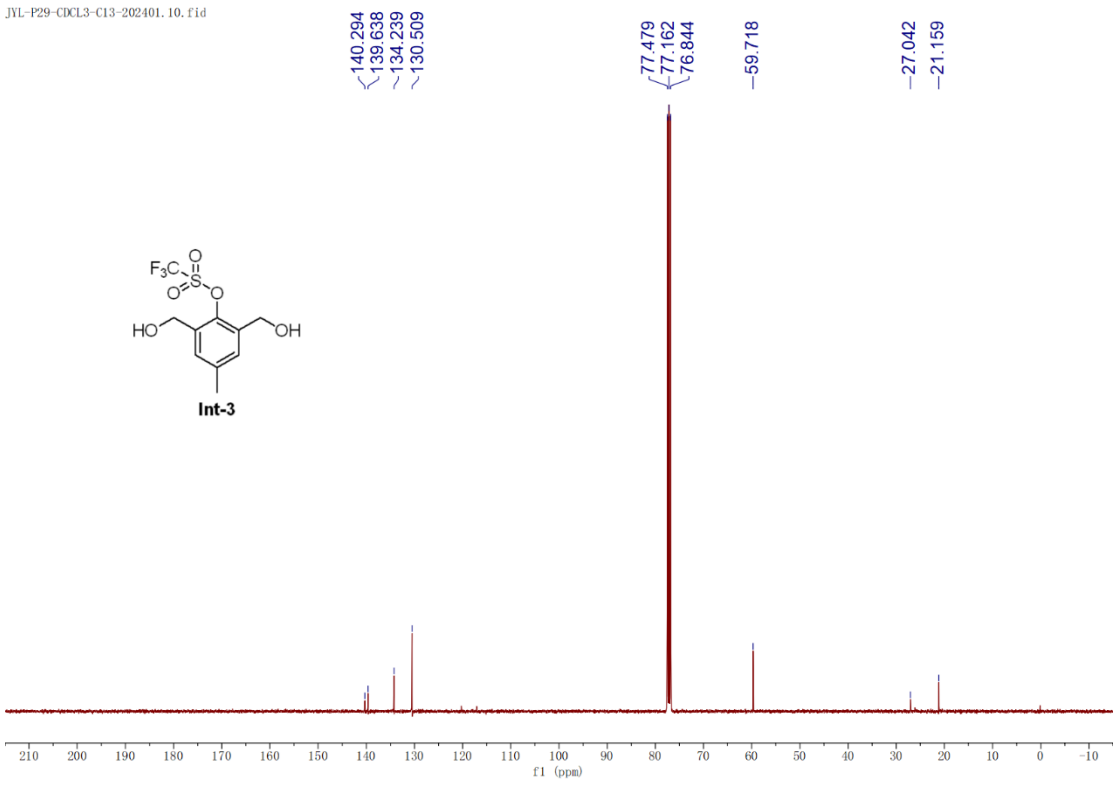

Figure S8. ^{13}C NMR spectrum of Int-3.

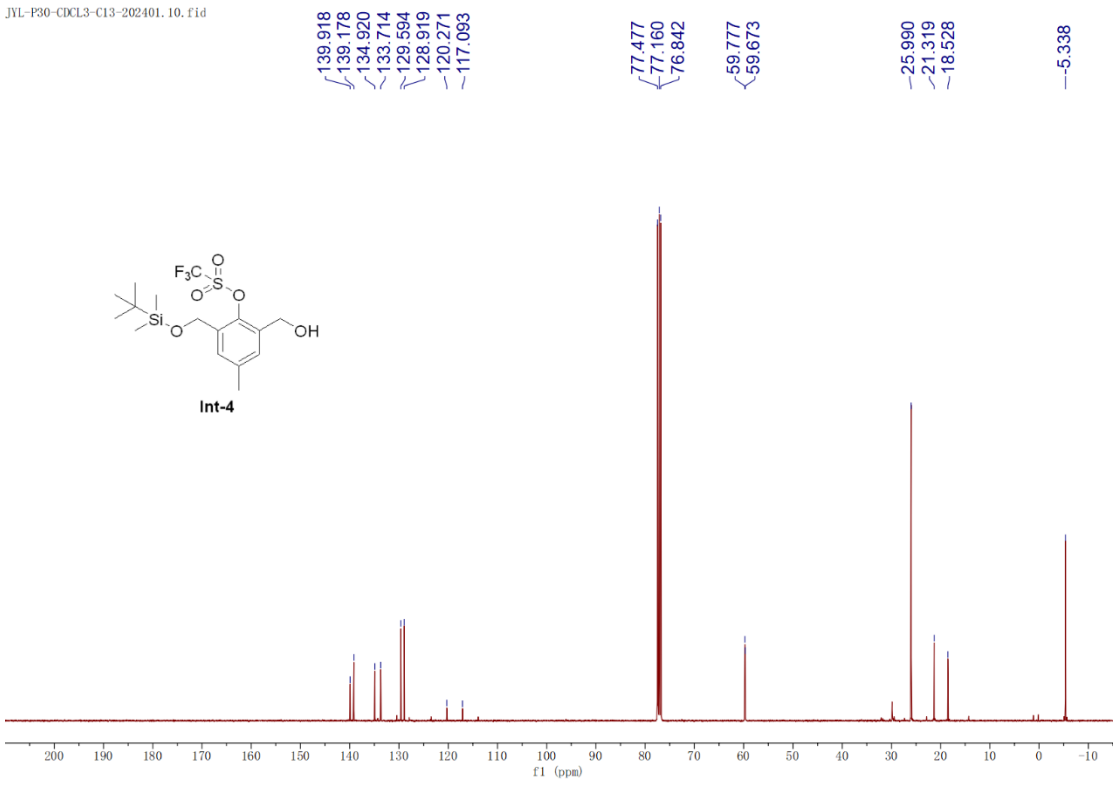

Figure S9 ^{13}C NMR spectrum of Int-4.

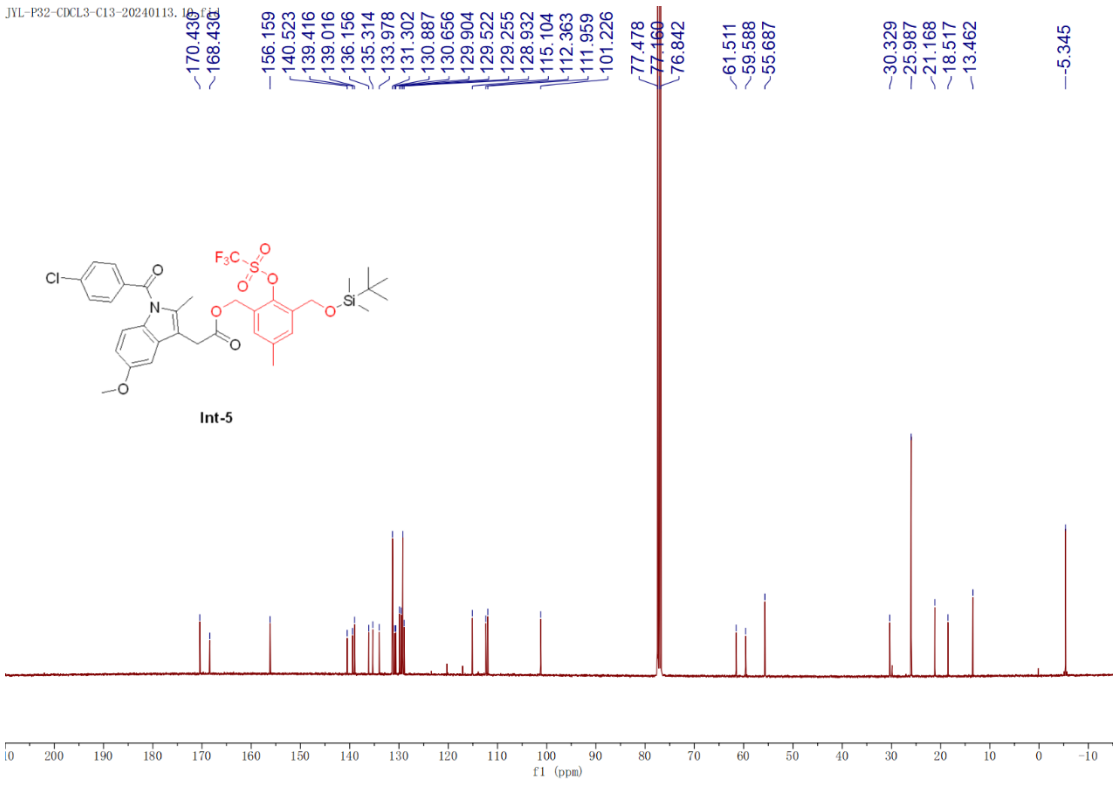

Figure S10 ^{13}C NMR spectrum of Int-5.

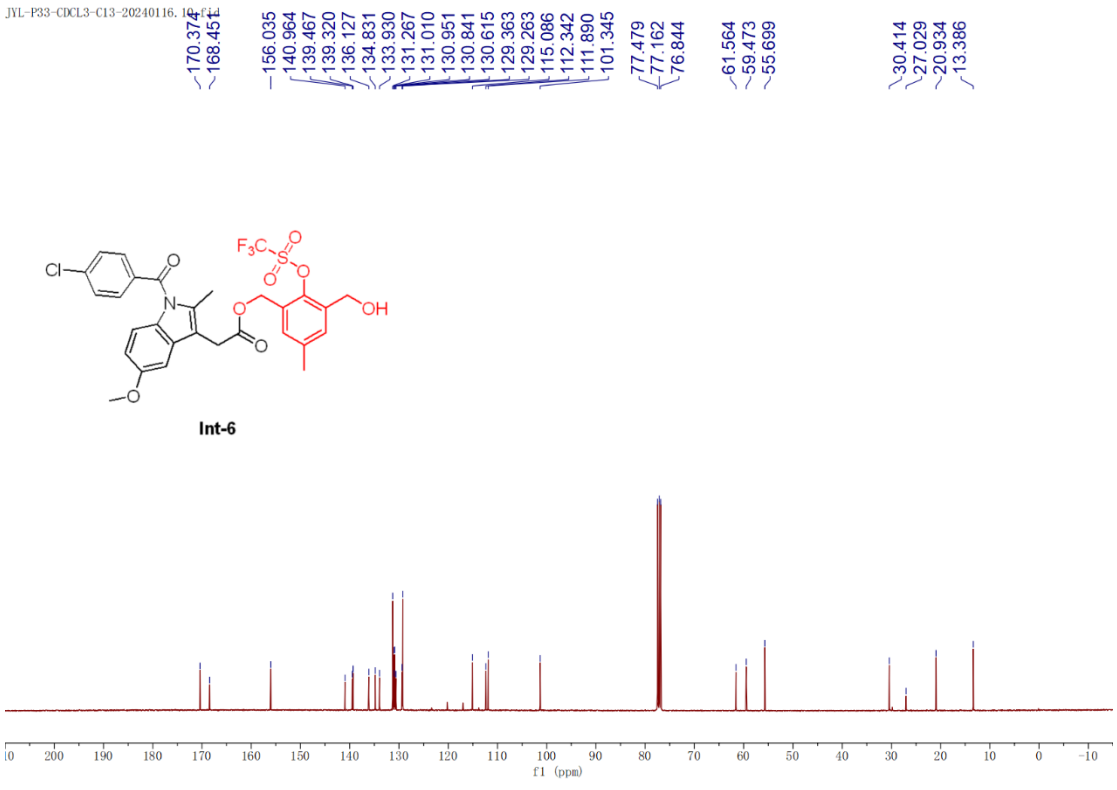

Figure S11 ^{13}C NMR spectrum of Int-6.

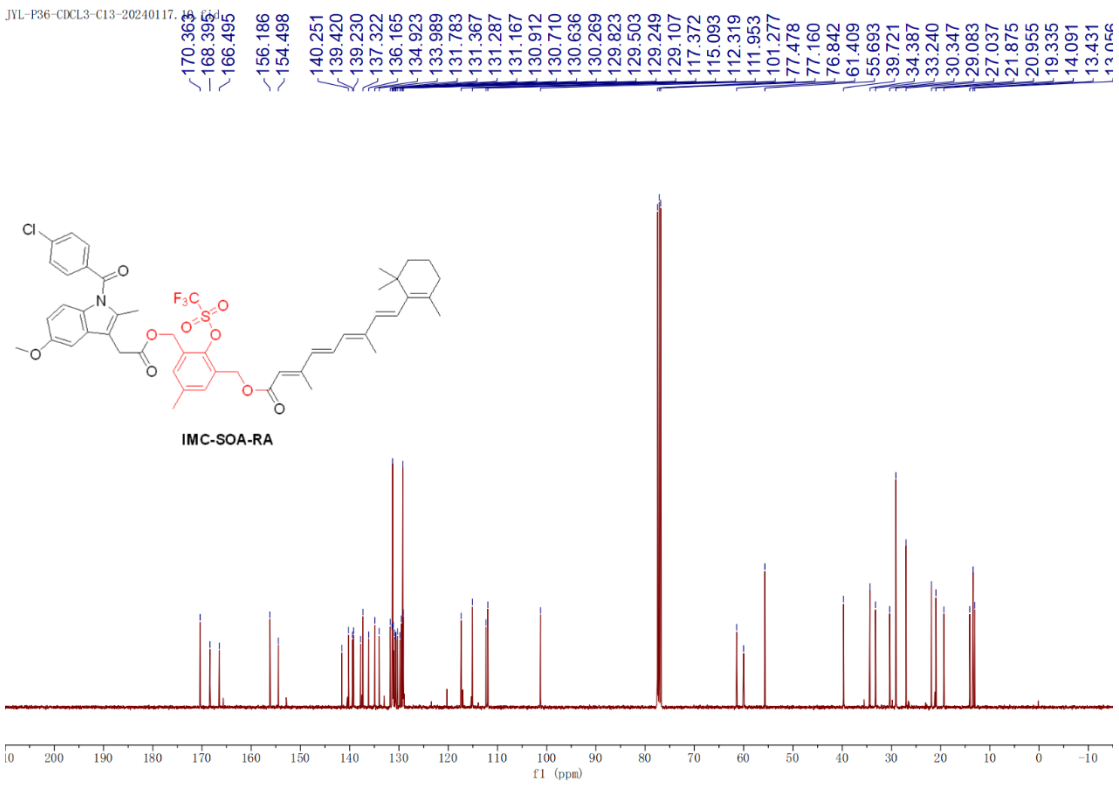

Figure S12 ^{13}C NMR spectrum of ISR.

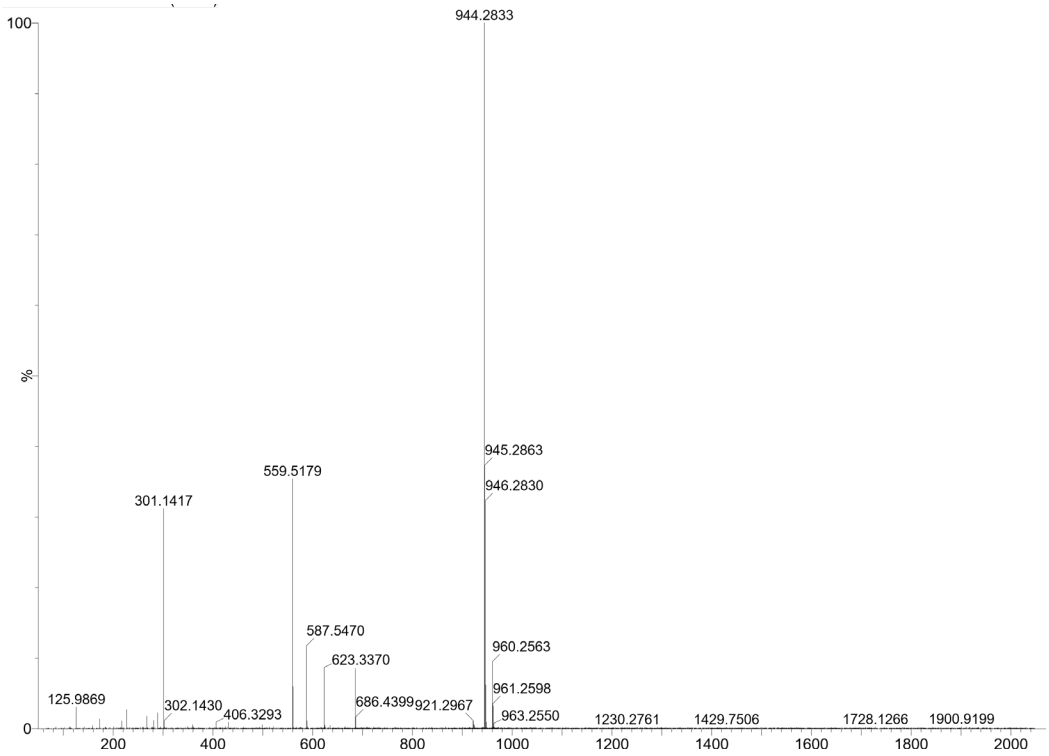

Figure S13 High resolution mass spectrum of ISR.

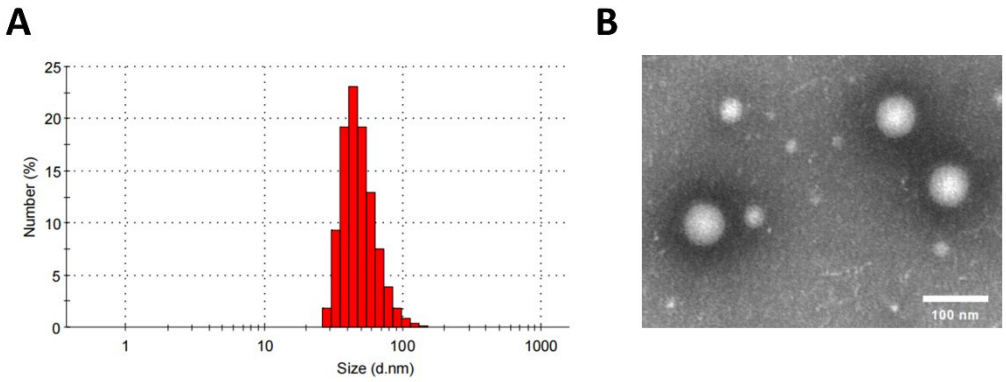

Figure S14 Size and TEM of DOX-ISR@HSA-DSPE. Scale bar: 100 nm.

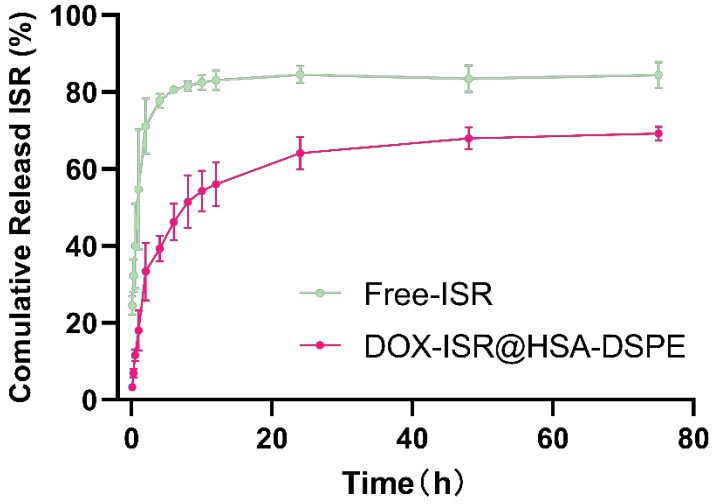

Figure S15 Schematic of ISR release profiles of Free-ISR and DOX-ISR@HSA-DSPE (*n* = 5). Data are mean ±SD.

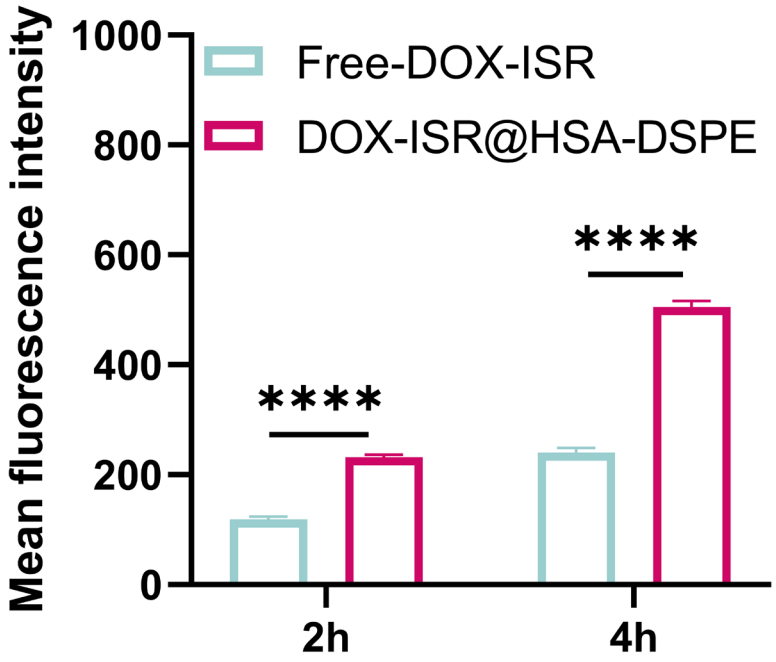

Figure S16 Statistical analysis of flow cytometry results (*n* = 3). Data are mean ±SD. ****p <0.0001.

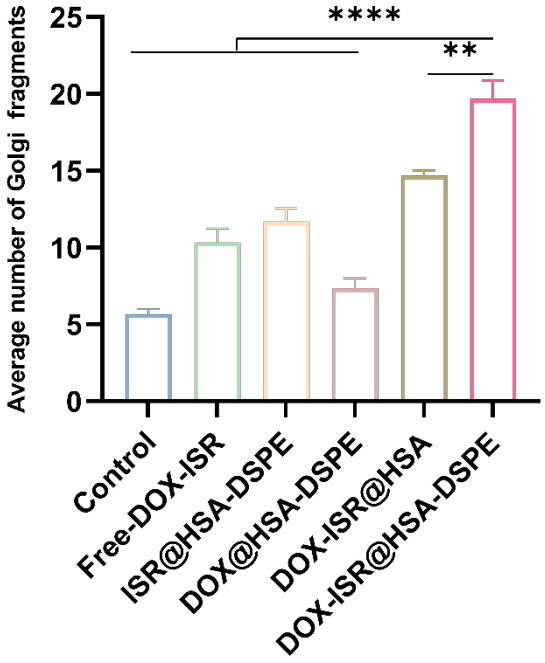

Figure S17 Quantification of Golgi fragments in 4T1 cells after different treatments by Image J (*n* = 3). Data are mean ±SD; **p < 0.01, ****p < 0.0001.

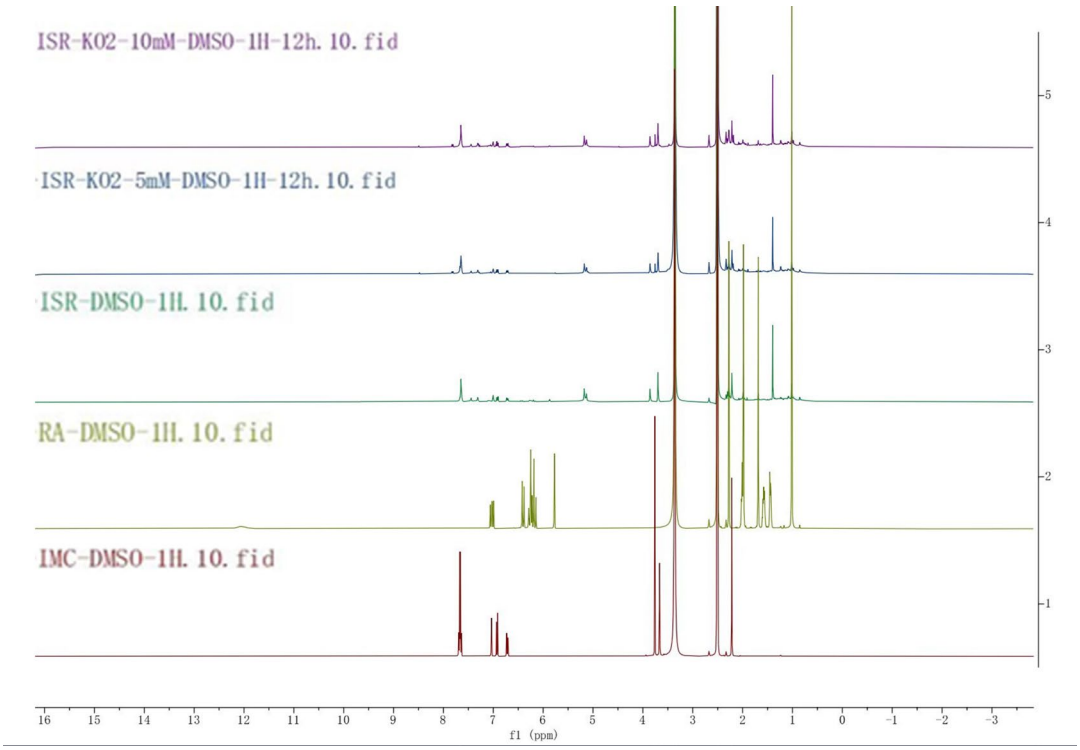

Figure S18 ^{1}H NMR spectra demonstrating ISR prodrug conversion to IMC and RA upon activation.

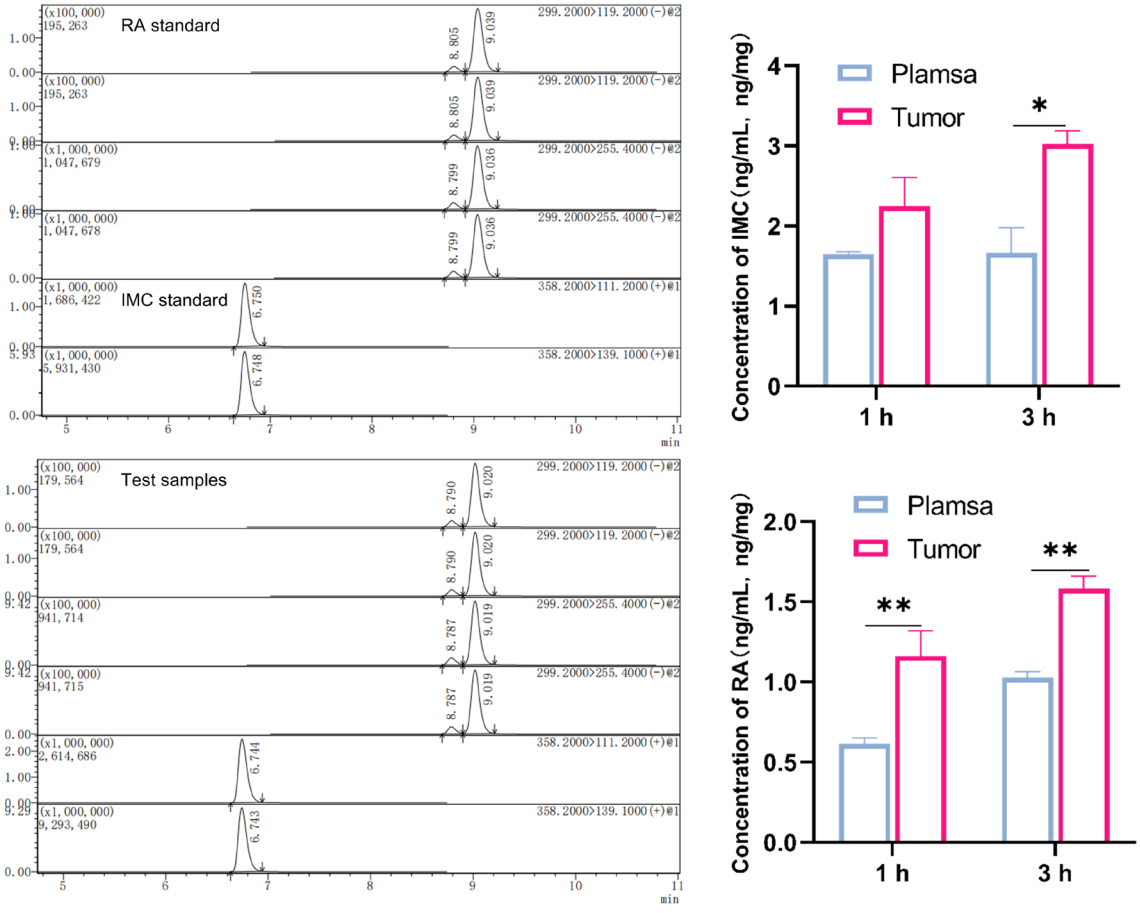

Figure S19 Post-Administration ISR Conversion to IMC and RA (LC-MS).

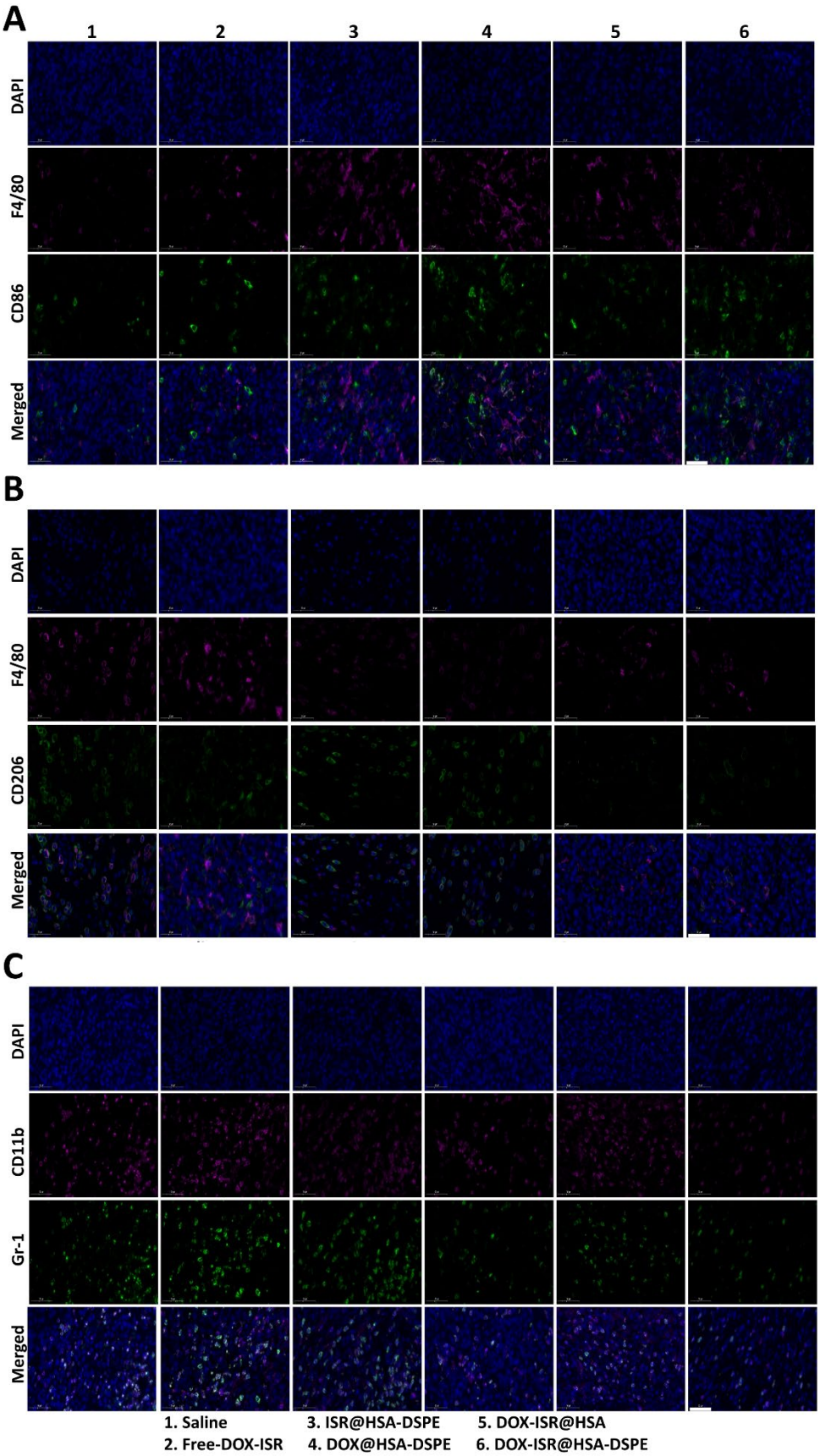

Figure S20 (A)F4/80$^+$ and CD86$^+$ staining of tumor tissues in each group (B)F4/80$^+$ and CD206$^+$ staining of tumor tissues in each group (C)CD11b$^+$ and Gr-1$^+$ staining of tumor tissues in each group, scale bar: 50 μm.

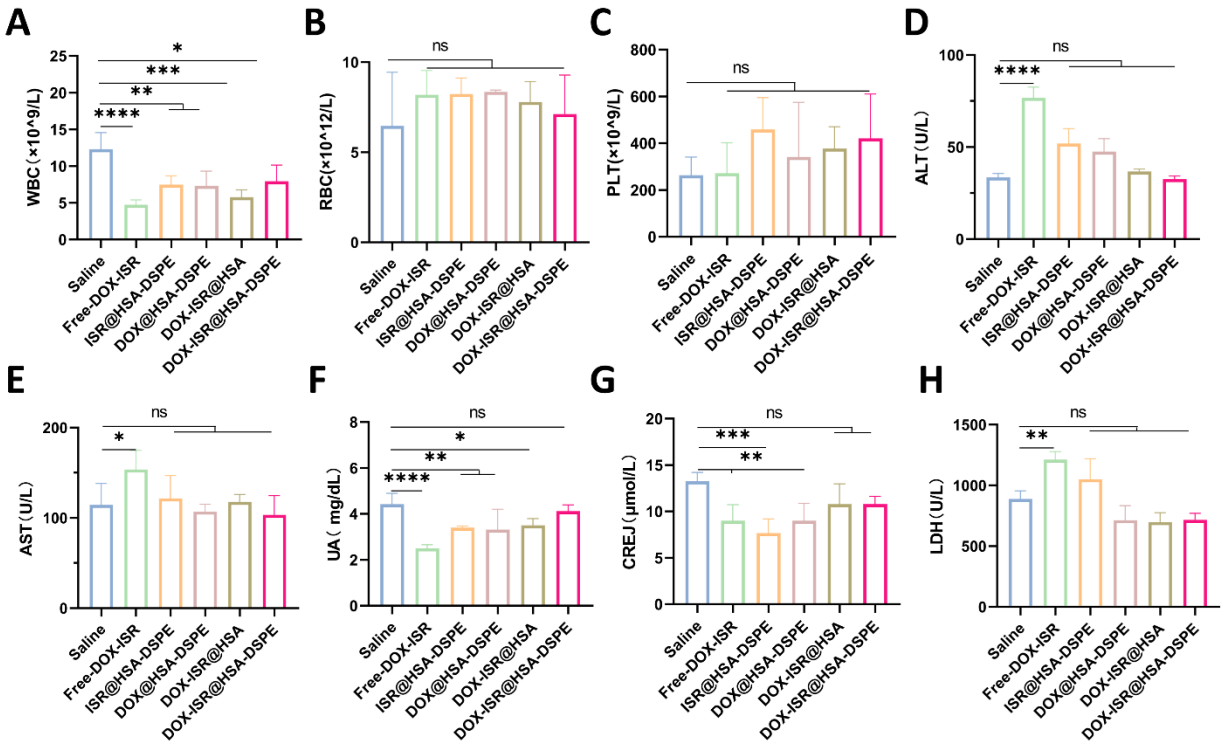

Figure S21 (A)-(C) Quantitative analysis of WBC (A), RBC (B), PLT (C) contents in mice (n = 5). (D)-(H) Blood biochemical analysis of the mice serum. ALT (D), AST (E), UA (F), CREJ (G), LDH (H) content quantitative determination results (n = 5). Data are mean ±SD; *p < 0.05, **p < 0.01, ***p < 0.001, ****p <0.0001, ns, not significant.